



Supplement of

Two subduction-related heterogeneities beneath the Eastern Alps and the Bohemian Massif imaged by high-resolution P-wave tomography

Jaroslava Plomerová et al.

Correspondence to: Jaroslava Plomerová (jpl@ig.cas.cz)

The copyright of individual parts of the supplement might differ from the article licence.

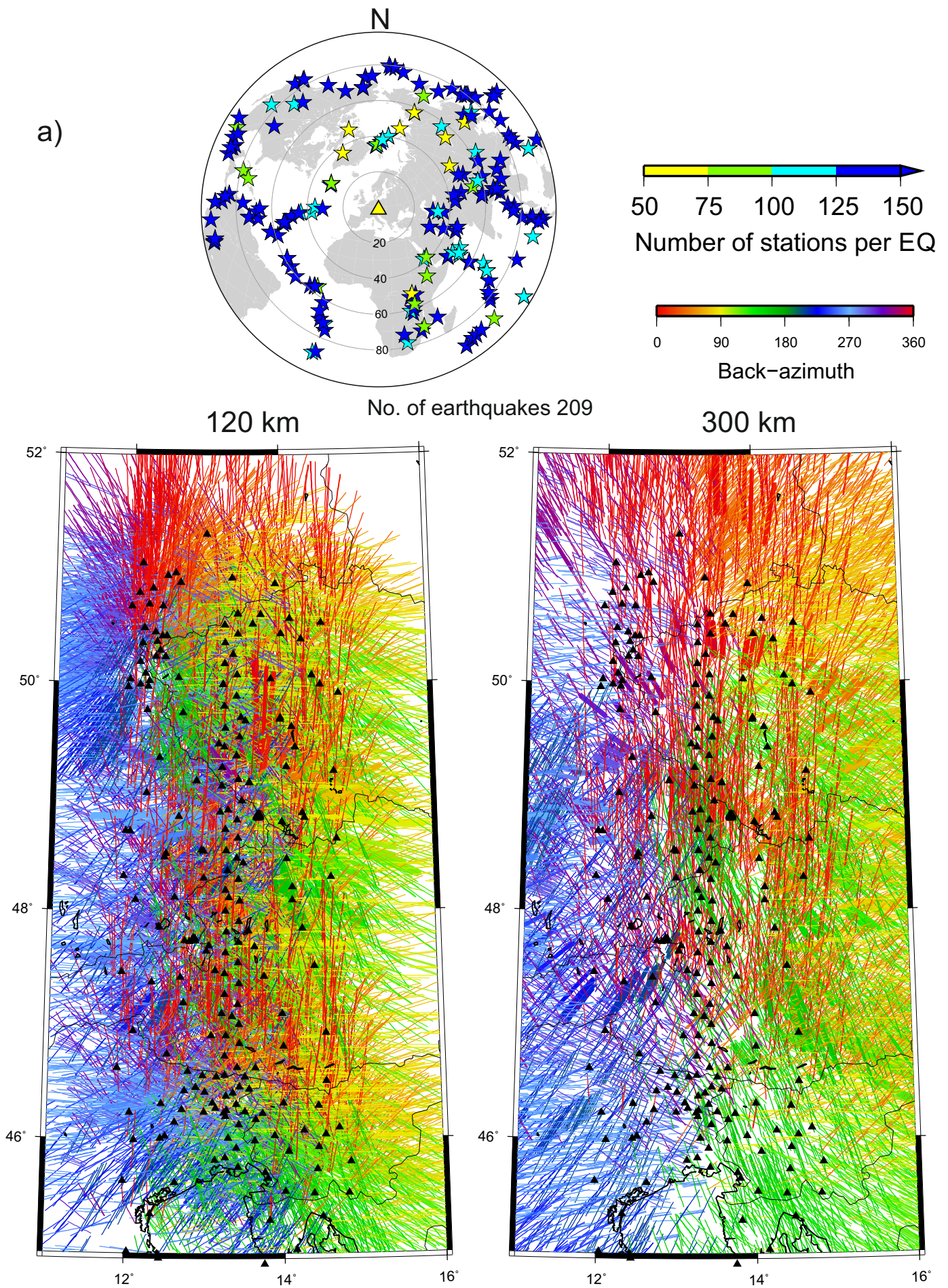


Figure S1: Distribution of teleseismic earthquakes used in the study and ray-path coverage (a). Distributions of extended set of earthquakes arriving from northern and southern back-azimuths in fans of 60° (b).

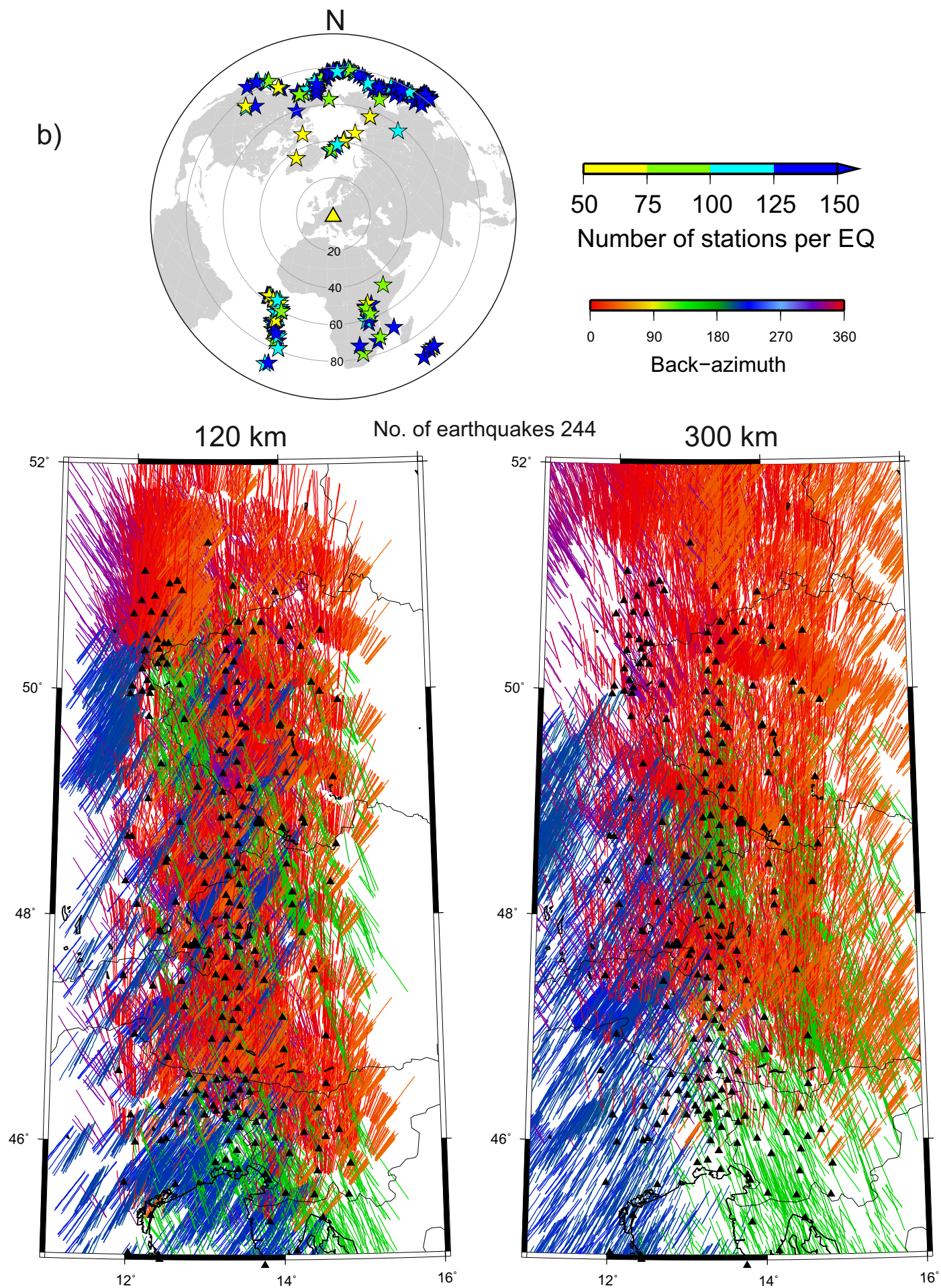


Figure S1: part b.

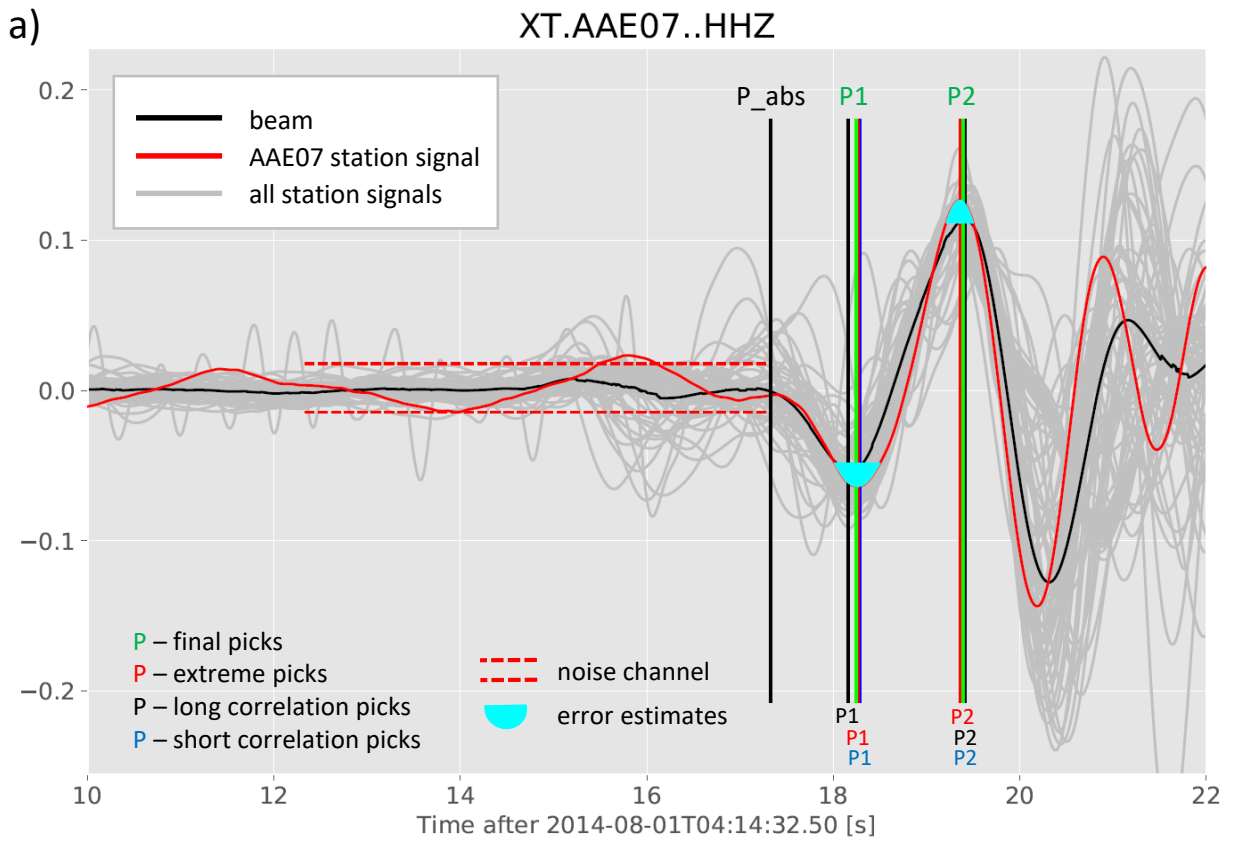


Figure S2a: An example of automatic measuring of P-wave arrival times. The TimePicker 2017 enables highly-accurate automatic measuring of absolute arrival times of teleseismic P-waves based on waveform cross-correlations and beam-forming. Assuming a waveform similarity of the teleseismic P-waveforms within an array, we cross-correlate and stack shifted traces of all the stations (grey traces), and create a low-noise beam trace of an event (black trace). Times of extremes on the station signal (red trace) are measured by three different methods. First, times of the station signal extremes are picked (red P1, P2). Second, we cross-correlate the station signal with the long P-waveform beam (~2.5 signal period) and determine the long correlation picks (black P1, P2). Third, we cross-correlate the station signal with the short P-waveform beam (~0.5 signal period) around each of the extremes and determine the short correlation picks (blue P1, P2). Each of the red, black and blue picks is complemented by its error estimate. Time error of the red extreme depends on a signal noise level (see cyan basins, their height is given by a noise magnitude - red dashed lines), errors of the black and blue correlation picks come from coherence of the signal with the beam. The final times of the extremes (green P1, P2) are probabilistic combinations of the three partial picks (red, black and blue P1, P2), which assures coherent measurements in case of more complex waveforms. The extreme with the lowest error estimate (green P2) is chosen for computation of the absolute arrival time of the P-wave at the station. For that we determine (1) the arrival time on the beam (P_abs) at a moment when the beam leaves its noise channel and (2) time of the beam extreme corresponding to the green P2 extreme. The time difference between them is then subtracted from the final time of the chosen station signal extreme (green P2).

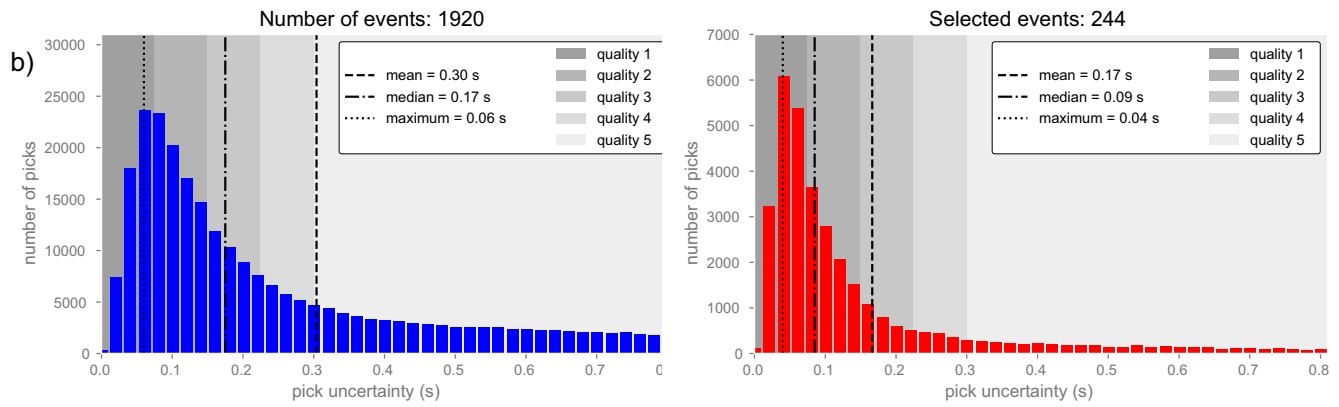


Figure S2b: Histograms of uncertainties of the full dataset (left panel) and of events selected for tomography (right panel). Mean and median of uncertainties, width of quality bins as well as uncertainty of the maximum of picks are indicated by vertical lines. The uncertainties are categorized into five quality classes ranging from 1 (the best) to 5 (the worst). Only arrival times measured with quality 1-3, with the mean 0.08s and median 0.07s, input the tomography.

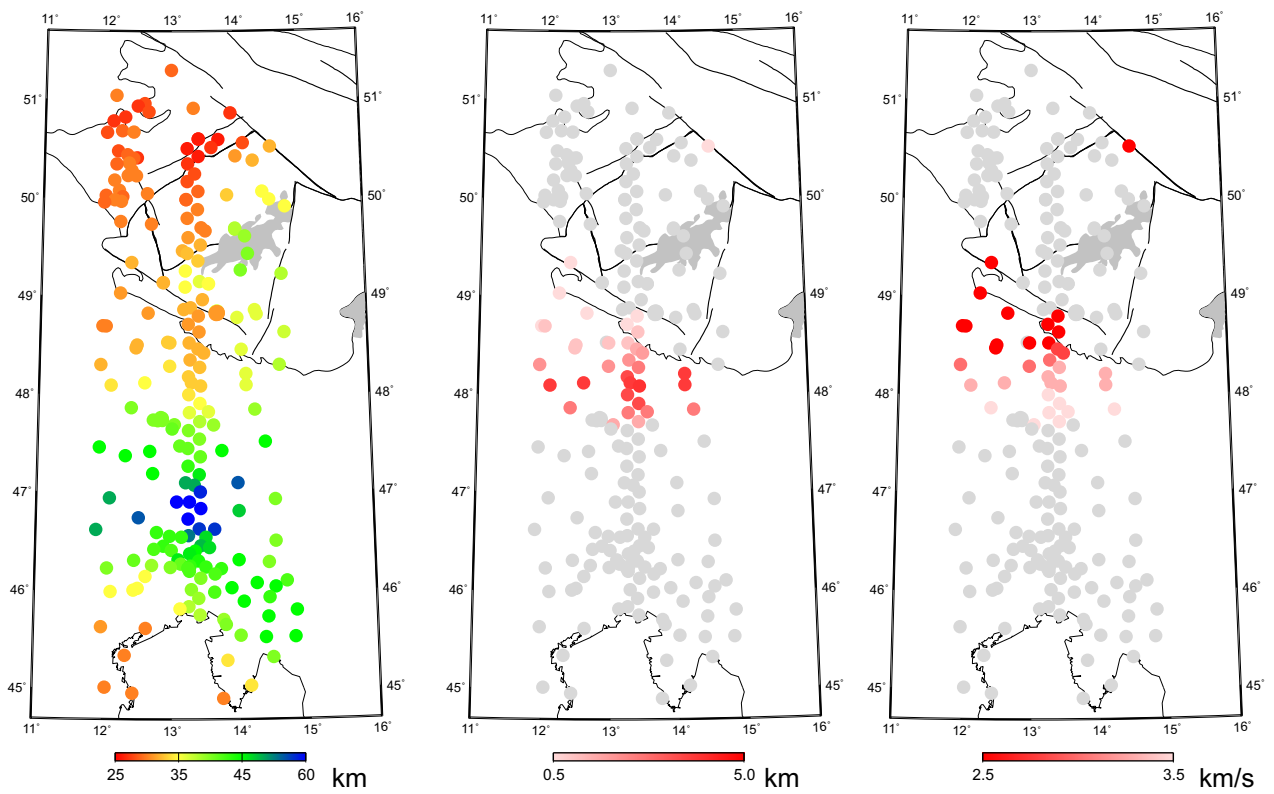


Figure S3: Maps of Moho depth (left) and thickness (center) and velocities (right) of sediments used to correct P-wave residuals for the crust relative to IASP'91 model.

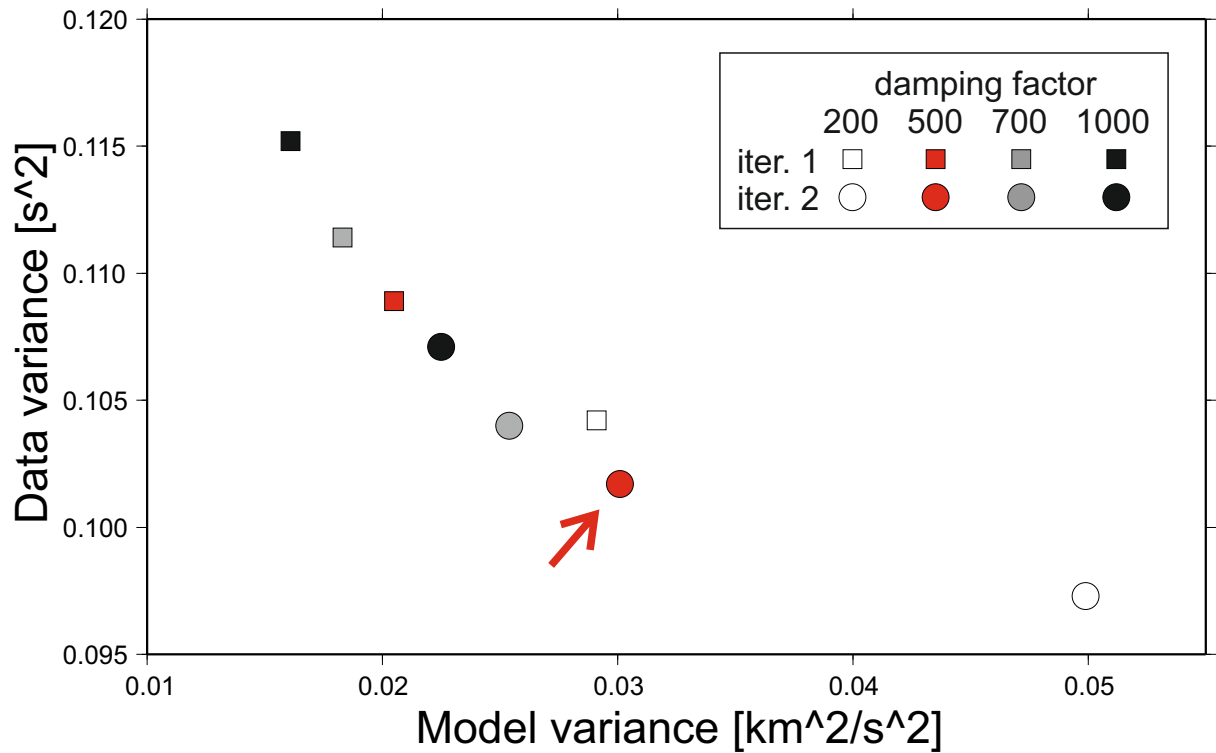


Figure S4: Data and model variance trade-off curve evaluated for various values of damping of the isotropic-velocity perturbations and numbers of iterations. Red arrow marks variances for the final model. The data variance and model variance are squared norms of the time residuals and velocity perturbations, respectively. The data uncertainties are included in the evaluation of the data variance. Data variance in the code is $1/(N-1) \cdot \sum((\text{residual} - \text{average of residuals}) \cdot \text{weight})^2$, i.e., instead of dividing by sigma, which is sometime used as well, the numerator is multiplied by a unitless weight.

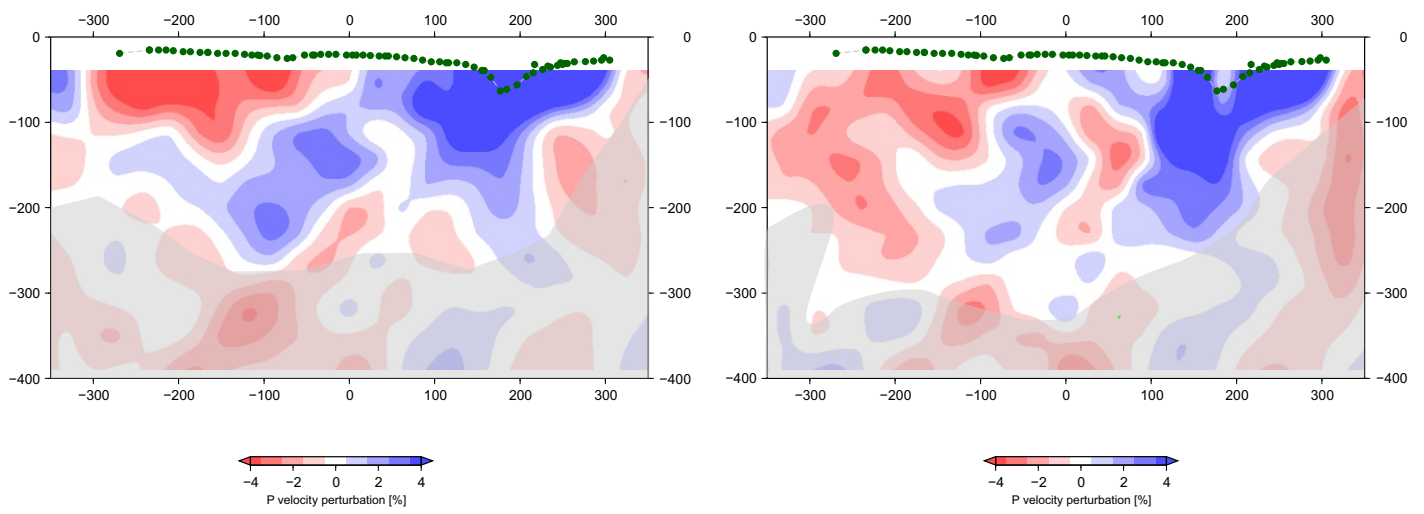


Figure S5: Velocity perturbations along Profile EASI through models calculated for rays from all directions (left) and for rays from the northern and southern 60° wide azimuth bins (right, see also Figs. 3 and S1). Relatively less-well resolved regions along the profile are shaded.

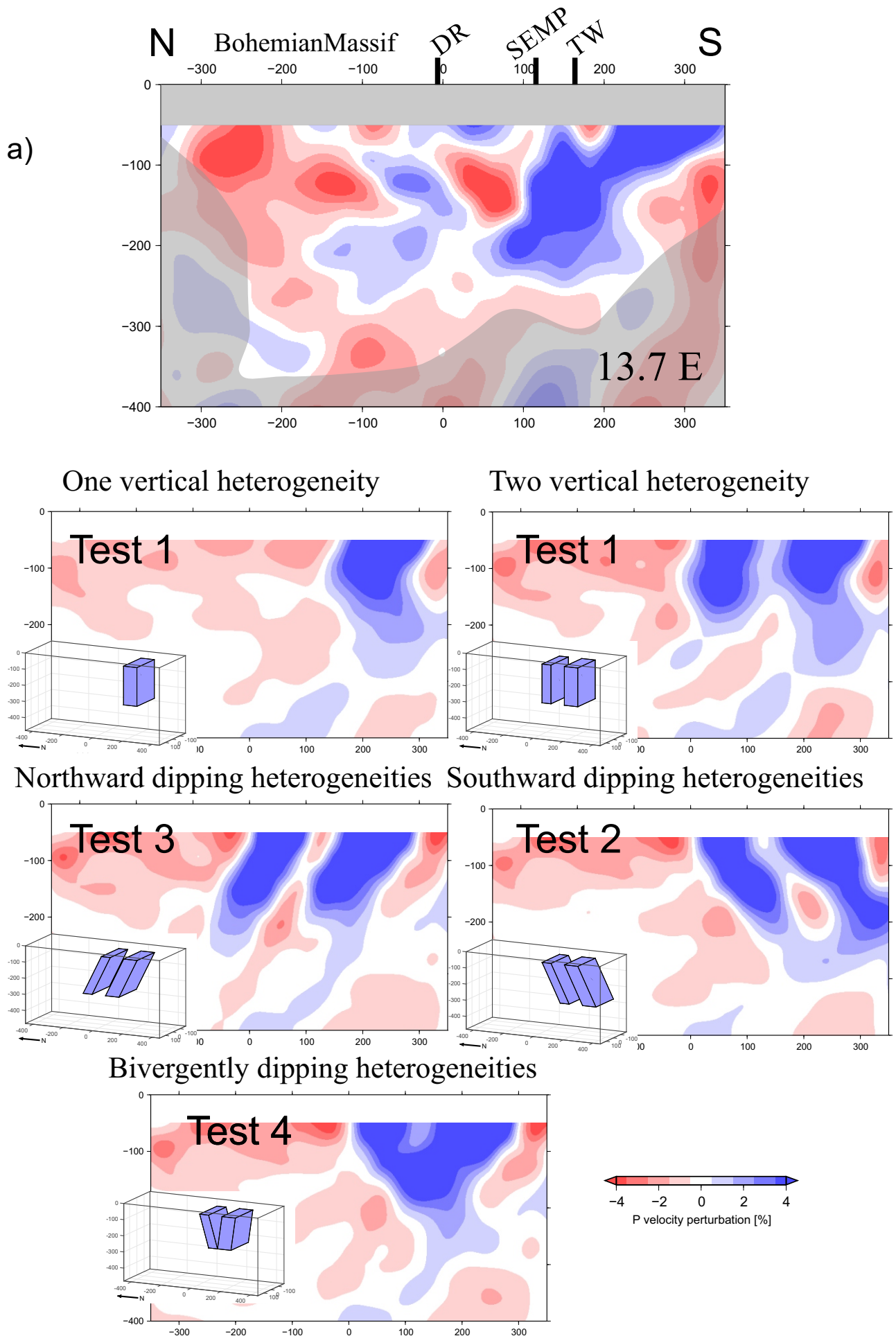


Figure S6: Synthetic tests of tomography capability to resolve one or two sub-parallel heterogeneities (TEST1) and their dip directions (TEST2, TEST3 and TEST4) in the north-south cross-sections parallel to the central EASI profile to its east (Figs. S6a,b) and west (Figs. S6c,d) corresponding to profiles of Figure 3.

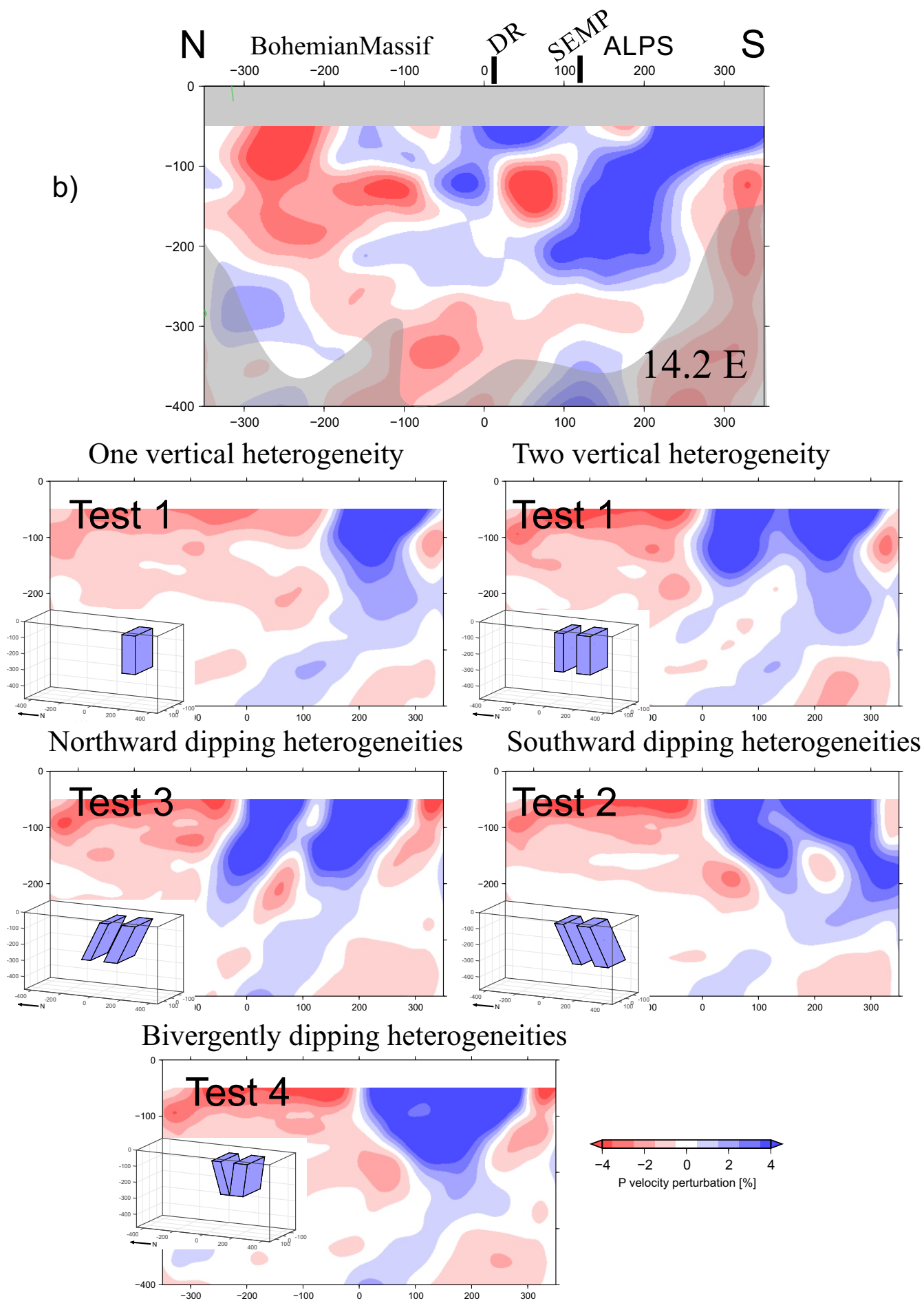


Figure S6: part b.

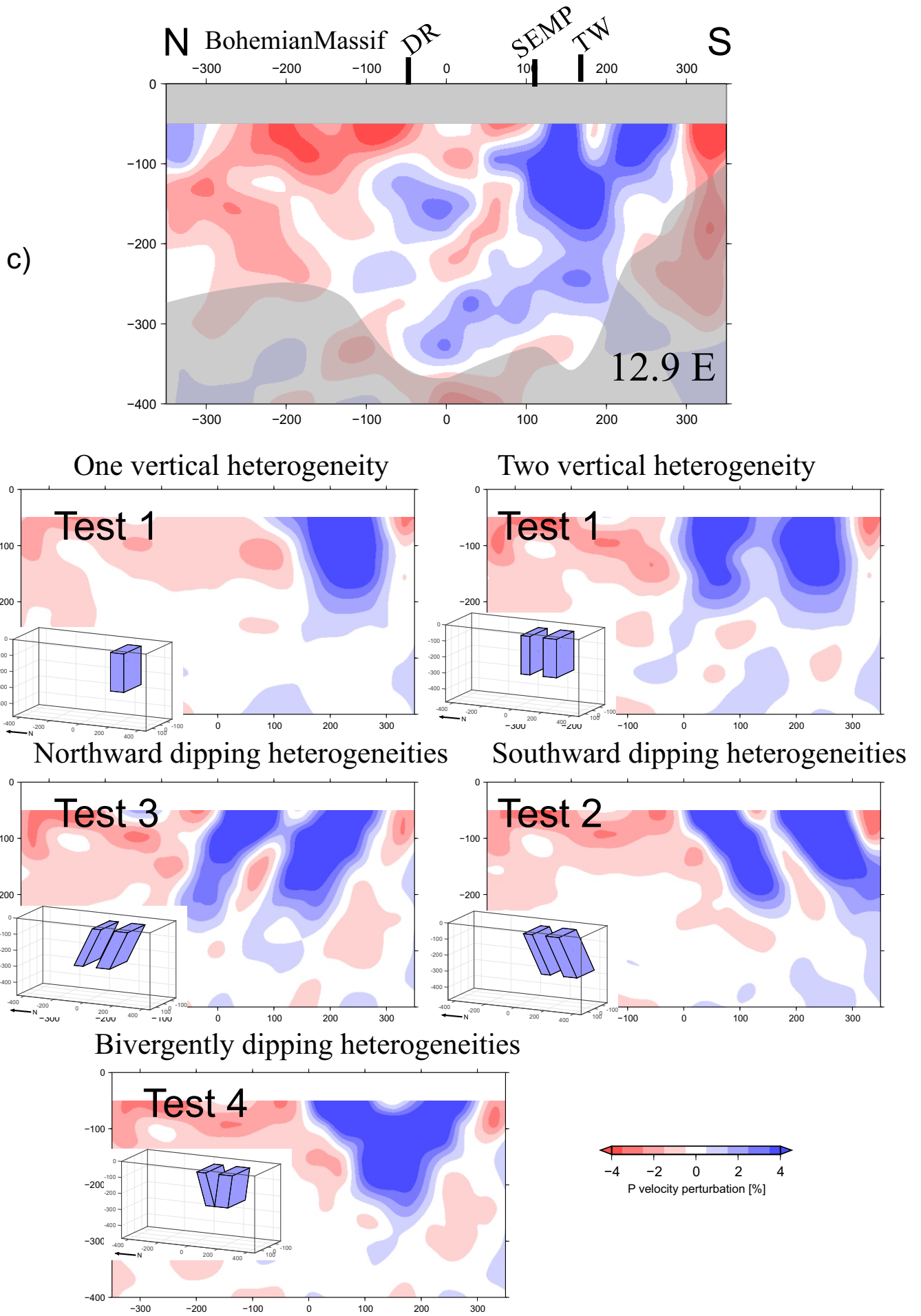


Figure S6: part c.

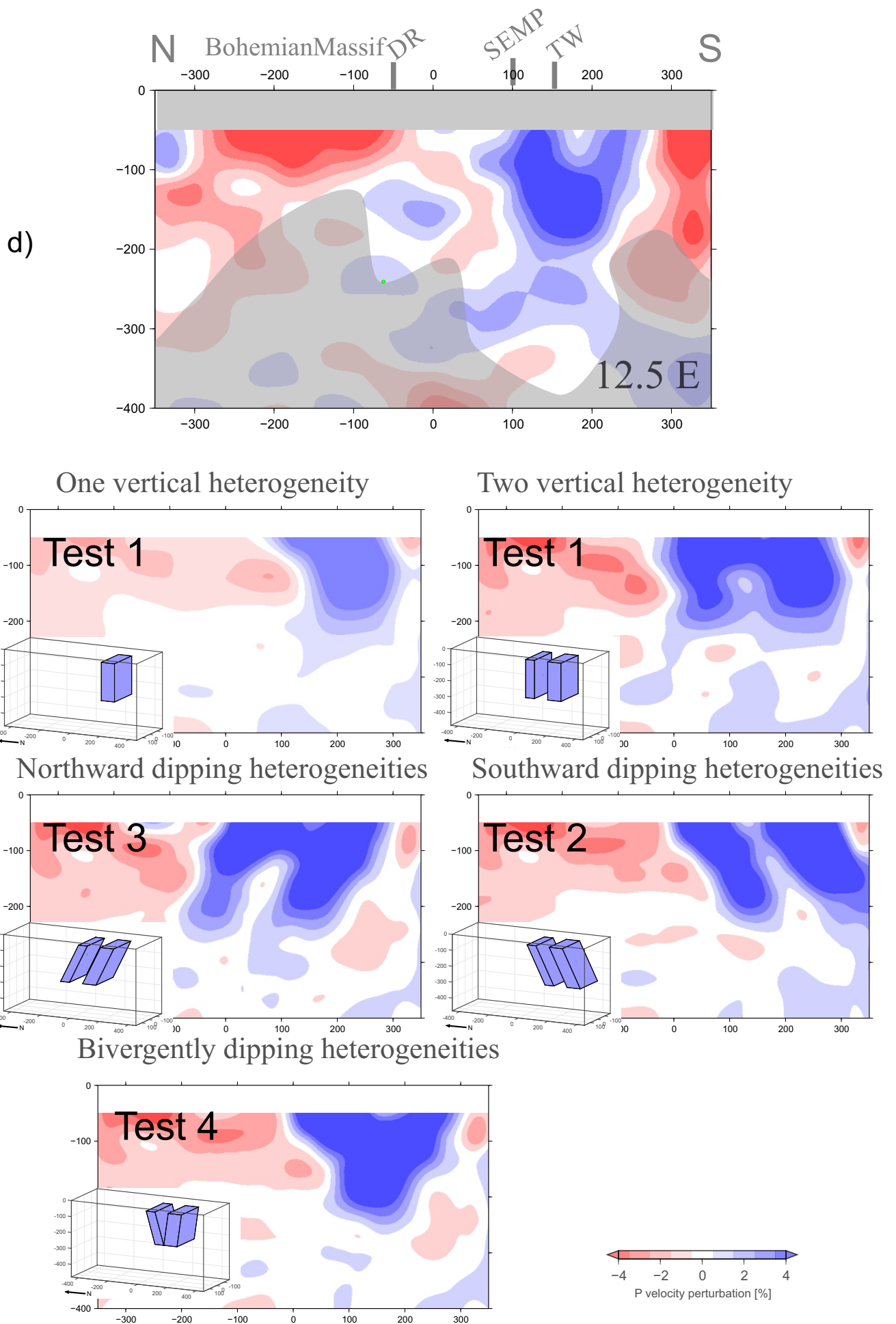


Figure S6: part d.

a)

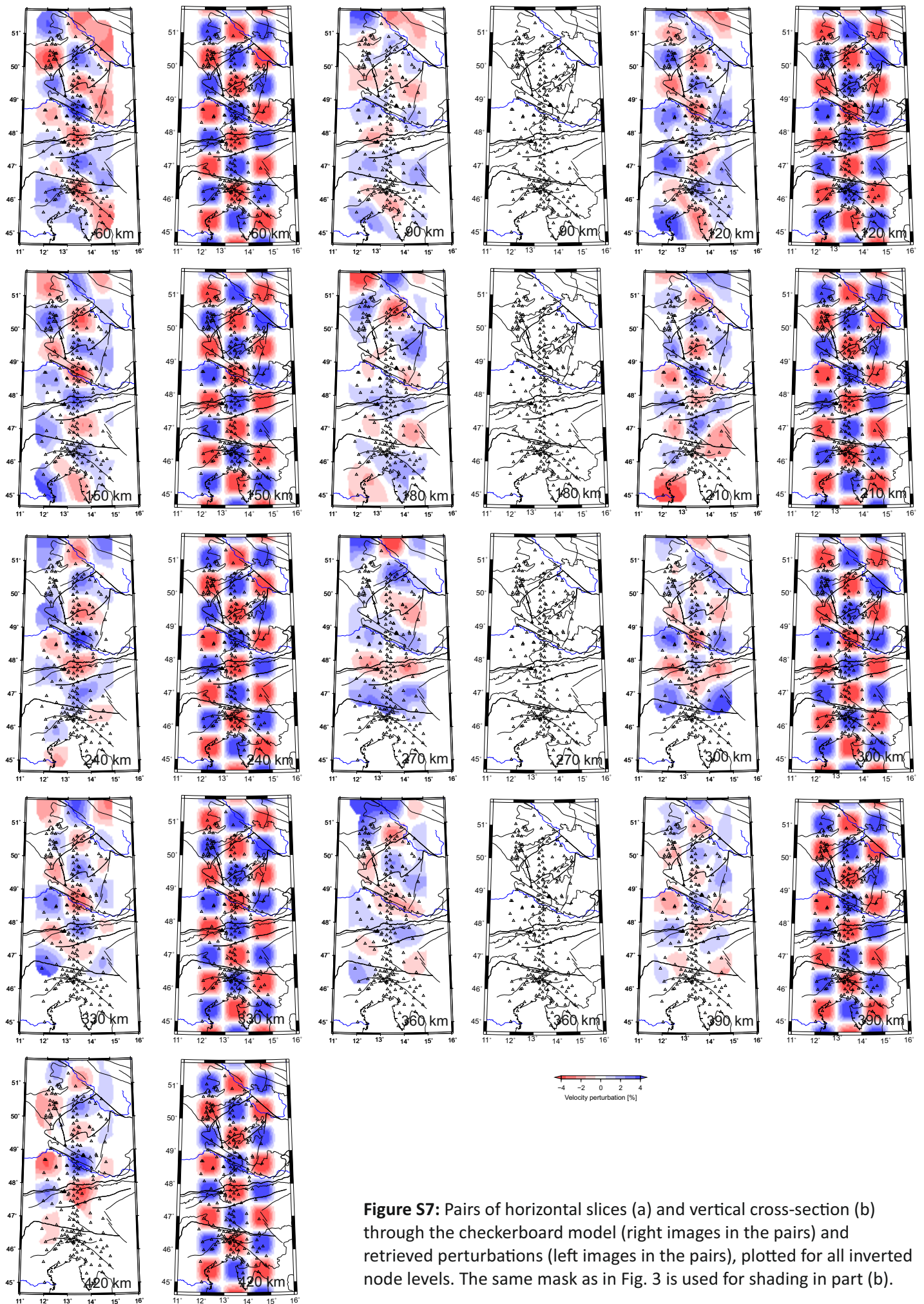


Figure S7: Pairs of horizontal slices (a) and vertical cross-section (b) through the checkerboard model (right images in the pairs) and retrieved perturbations (left images in the pairs), plotted for all inverted node levels. The same mask as in Fig. 3 is used for shading in part (b).

b)

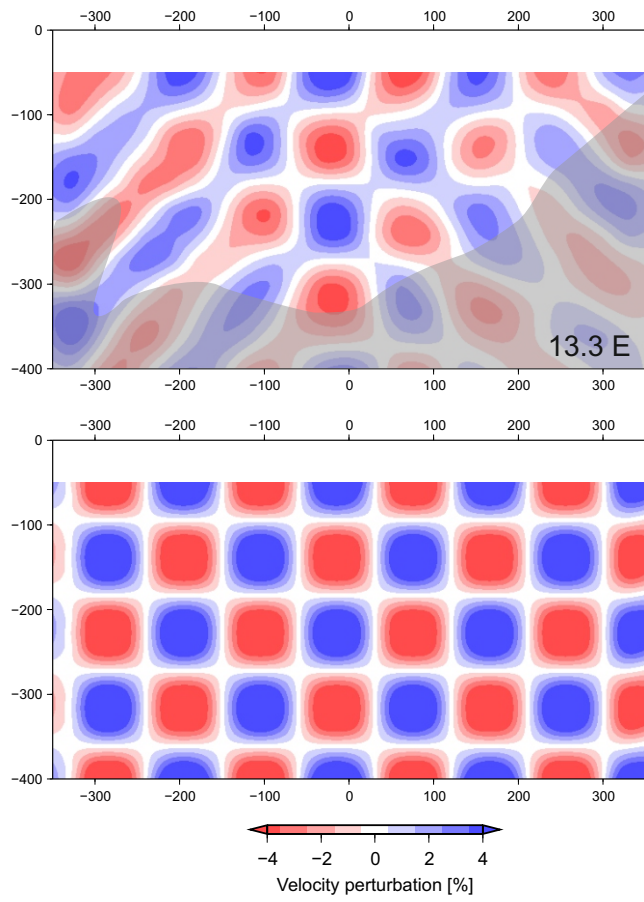


Figure 7: continuation, part (b)

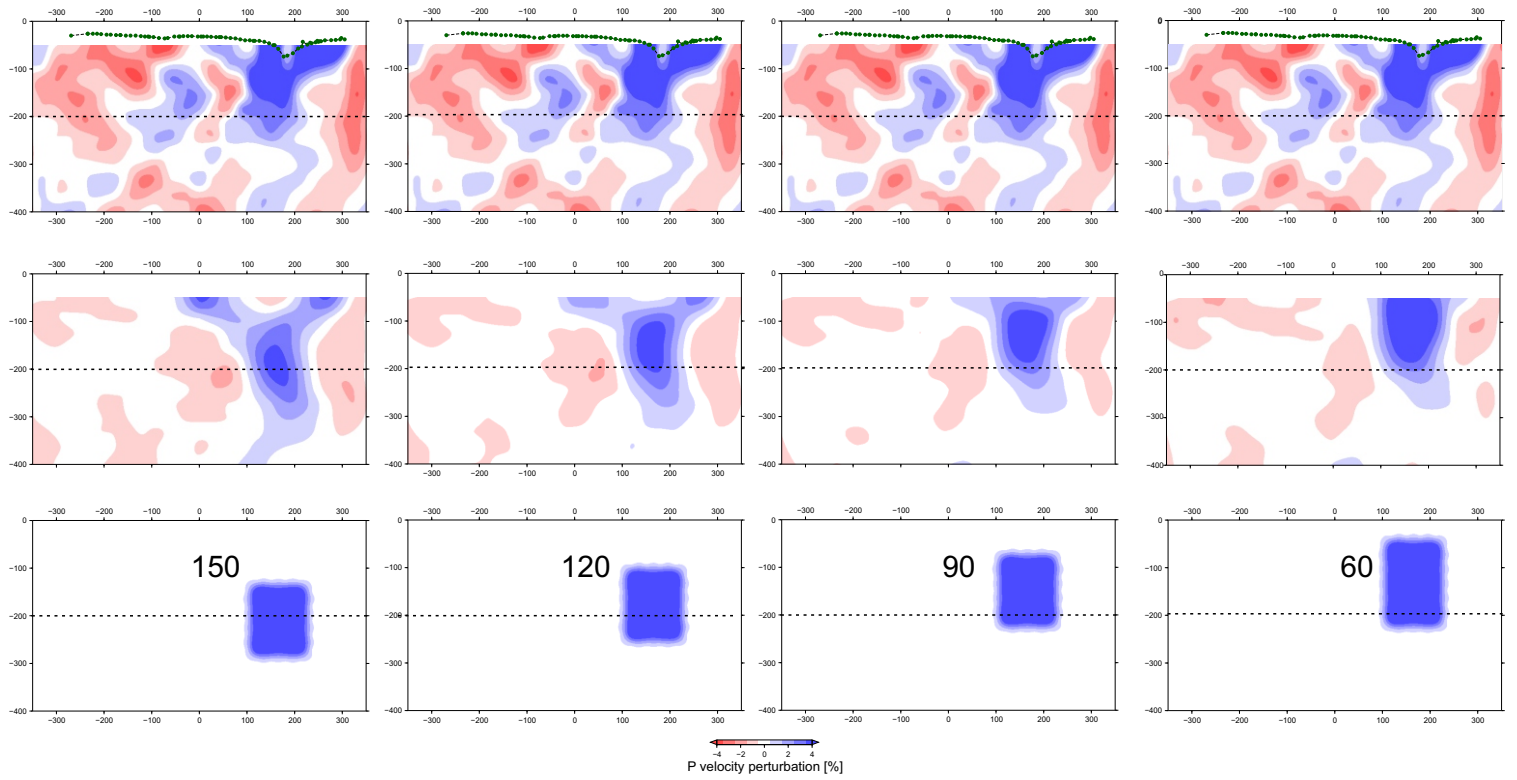
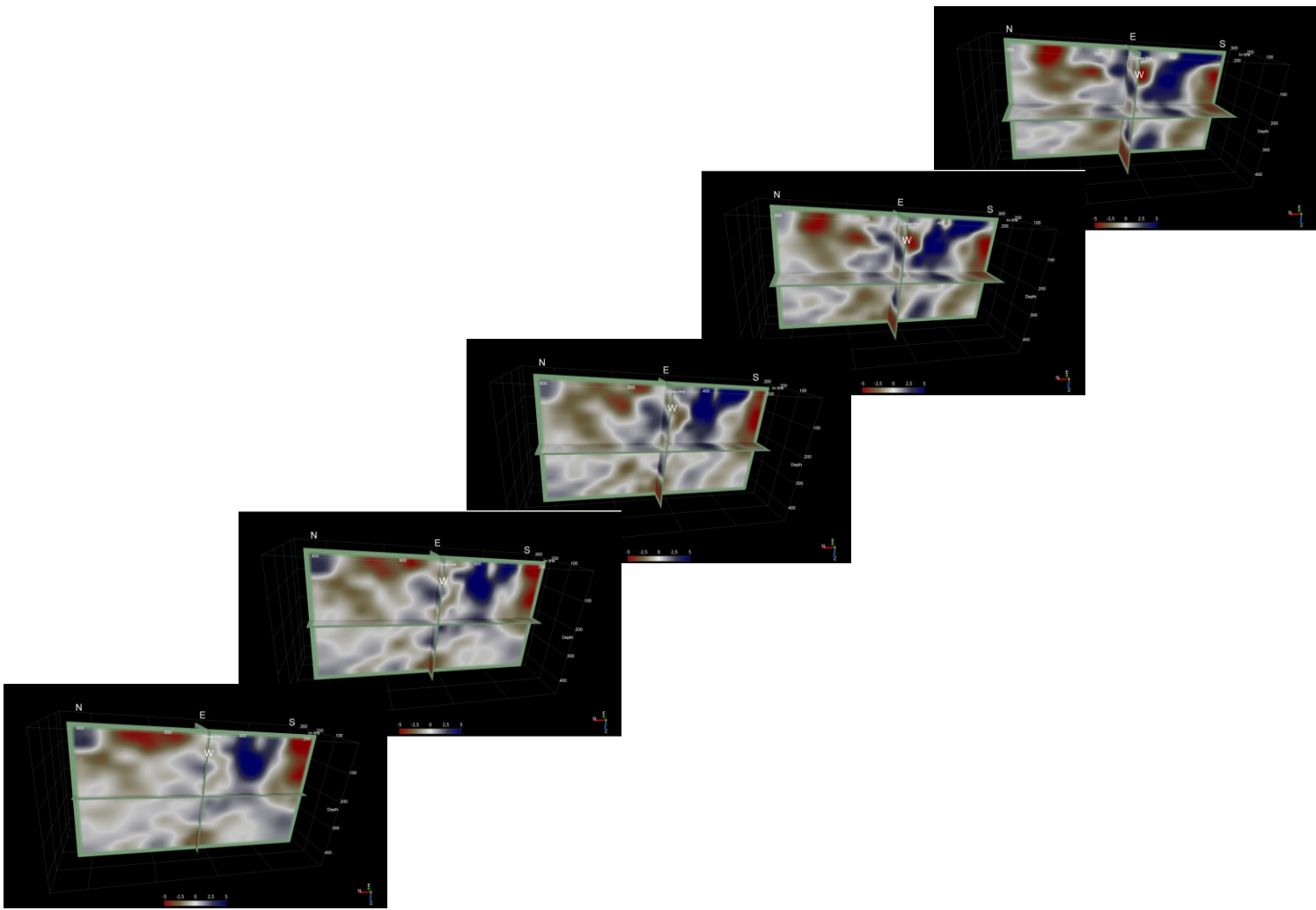


Figure S8: Velocity perturbations along the N-S cross-section in the center of the array from real data (upper row) and from synthetic data (middle row) calculated for models of the steep detached slab beneath the E. Alps (lower row). The top of the heterogeneity migrates upward (bottom row) from 150 km (detachment as in Paffrath et al., 2021) to 60 km (representing no detachment). The slab detachment larger than the 30km grid would be revealed in the upper 200 km of the EASI-AA model. A potential leakage does not overprint the images.

Eastermost cross-section



Westernmost cross-section

Figure S9: Cross-sections through a 3D visualization of along-strike changes of the velocity perturbation in the EASI-AA model.